Measurement of the absolute penetration depth and surface resistance of superconductors and normal metals with the variable spacing parallel plate resonator

Vladimir V. Talanov,[a] Lucia V. Mercaldo,[b] and Steven M. Anlage
Center for Superconductivity Research, Department of Physics, University of Maryland, College Park, Maryland 20742

John H. Claassen
Naval Research Laboratory, 4555 Overlook Avenue, S.W., Washington, DC 20375

(Received 27 July 1999; accepted for publication 24 January 2000)

The variable spacing parallel plate resonator (VSPPR) is a microwave transmission line resonator with a continuously variable thickness of the dielectric spacer between the superconducting or metallic plates, filled by cryogenic liquid or vacuum. We measure the dielectric spacer thickness dependencies of the resonator frequency and quality factor, and fit them to theoretical forms, in order to extract the absolute values of penetration depth, λ, and surface resistance, R_s. A cryogenic micropositioning setup is developed to vary the spacer thickness from 0 to 100 μm with a resolution of 8.5 nm, and to maintain parallelism of the resonator plates. Measurement of ac capacitance between the plates is utilized to directly determine the separation between the resonator plates and to reduce the effect of their tilt and nonflatness on the accuracy of the measured R_s and λ. Because the operating temperature is fixed (77 K), the result for a superconductor is independent of an *a priori* model for the penetration depth versus temperature. This technique can also be employed as a surface impedance standard for characterization of high temperature superconducting films for microwave applications. © *2000 American Institute of Physics.* [S0034-6748(00)03605-4]

I. INTRODUCTION

A. Why measure the absolute penetration depth and surface resistance?

In the last decade, great progress in the investigation of the microwave surface impedance $Z_s=R_s+iX_s$ of superconductors has been achieved. This progress, based on the pioneering works of Pippard[1] and others, was reinvigorated by the discovery of high temperature superconductivity (HTS).[2,3] An additional impetus for the development was the appearance of a new family of synthesized microwave sources and network analyzers, which enabled many novel techniques to be developed[4–9] (see also references in Sec. I B). Most of them give accurate determinations of the absolute value of the surface resistance, R_s, and provide very sensitive measurements of changes in the surface reactance $X_s=\mu_0\omega\lambda$ or the magnetic penetration depth λ. However, it is still a problem to experimentally determine the absolute value of λ because it is rather small—on the order of tens to hundreds of nanometers. In fact, unlike R_s measurements, today there is no well-established universal and commonly accepted technique for determination of the absolute penetration depth in superconductors.

Investigation of superconducting surface impedance is important because it yields valuable information about intrinsic (charge carrier density, pairing state symmetry, quasiparticle excitation spectrum, and relaxation time) and extrinsic properties (microstructure) of the specimen under study. These properties can be deduced from the surface impedance $Z_s=\sqrt{i\mu_0\omega/\sigma}$ (local limit) measured as a function of temperature, applied magnetic field, doping, or impurity concentration. Here, the complex conductivity, $\sigma=\sigma_1-i\sigma_2$, is a fundamental quantity which theories of superconductivity are able to calculate.[10,11] However, the inability to determine both the surface resistance and the absolute value of λ for the same sample often hampers the effort to construct the complex conductivity from the surface impedance data. For instance, the real part of the conductivity σ_1 can be extracted from R_s only if the absolute λ is available.[12]

The appearance of low loss HTS epitaxial thin films on single-crystal dielectric substrates has led to a rapidly growing field of superconducting wireless communication. Here, a knowledge of the surface impedance is important to get the optimum performance of superconducting rf/microwave components and circuits.[4,6,13] Another important issue is the establishment of a standard characterization technique for HTS thin films for microwave applications.[14]

B. How to measure the absolute penetration depth?

Though various experimental methods have been developed to study the magnetic penetration depth in superconductors (usually thin films or single crystals),[7,8,12,15,16] only a few of them are suitable for measurement of the absolute λ. They may be divided into the following four categories: ab-

[a]Present address: Neocera, Inc., 10000 Virginia Manor Road, Beltsville, MD 20705. Also at Institute for Physics of Microstructures of the Russian Academy of Sciences, Nizhny Novgorod, Russia.
[b]Also at Dipartimento di Fisica, Università degli Studi di Salerno, Baronissi, Salerno I-84081, Italy.

solute length scale techniques, reflection or transmission measurements of electromagnetic fields [mutual inductance, microwave/millimeter wave, infrared (IR) spectroscopy], measurement of internal magnetic field distribution (muon spin rotation [μSR], neutron scattering), and Josephson tunneling experiments.

1. Absolute length scale techniques

These techniques are generally based on the effect of electromagnetic field exclusion in the Meissner state of a superconductor. For single crystals, these include dc/ac magnetometry[17] and rf/microwave resonator perturbation techniques.[8,9,18] In all of them, an absolute length scale l is the specimen's linear dimension and the measured signal (for example, shift in the resonant frequency between the empty and perturbed resonator) is proportional to $(l-\gamma\lambda)\times$(area of the sample), where $\gamma\sim 1$ depends on the sample geometry and the field configuration. Usually, for crystals $\lambda/l \sim 10^{-3}-10^{-4}$ and the relevant calibration does not allow one to measure an absolute λ. In the case of a resonator in which all or a substantial part of it is made up of the superconductive material, $l=\Gamma/\mu_0\omega$, where Γ is the so-called resonator geometrical factor. The resonant frequency is $f_{SC} \simeq f_0(1-\lambda/2l)$, where f_0 is the frequency of the same perfectly conducting resonator. Cavity-like resonators, such as end-plate[19] or dielectric resonator[20–22] have l on the order of the wavelength of electromagnetic radiation and the ratio $\lambda/l \leqslant 10^{-4}$ is rather small. Planar resonators, such as stripline[23–25] or conventional parallel plate,[26–38] carry a slowed-down electromagnetic wave with the phase velocity $c_{sw}=c/\sqrt{\epsilon_{eff}(1+2\lambda/s)}$,[39] where c is the light velocity in vacuum, ϵ_{eff} is the effective dielectric constant of the transmission line, and s is the dielectric thickness. They have a high sensitivity to the penetration depth (down to 0.1 nm), because $\lambda/l=2\lambda/s\sim 10^{-2}-10^{-4}$ in this case. However, neither the cavity-like nor planar resonators are suitable for direct measurement of absolute λ (except possibly for the coplanar resonator[40,41]), and only changes in λ may be extracted from the experiment.

The only possible (and commonly used) way to evaluate an absolute $\lambda(T=0)$ using the above techniques involves fitting of the measured temperature dependence of the parameter relevant to the changes in λ (commonly, shift in the resonant frequency) to a theoretical dependence for $\lambda(T)$. Usually, this procedure works properly for conventional superconductors where appropriate models (two fluid or BCS) for $\lambda(T)$ are well established. However, such models fail in the presence of extrinsic effects in the sample under study. In the case of HTS, there is a lack of suitable models for $\lambda(T)$, and usually the absolute λ values deduced from experiment are strongly dependent (up to 50%) on the form of the temperature model assumed.[16,42,43]

The other three categories of techniques generally allow one to measure absolute λ without the need to determine the absolute length scale. When combined with techniques of measuring the surface impedance, they allow one to reconstruct the complex conductivity σ.[8,12]

2. Reflection/transmission of electromagnetic field

The mutual inductance technique[44–46] is based on a measurement of the mutual ac inductance of two axially symmetric coils separated by a superconducting film. This technique is accurate for film thickness up to 1 μm for typical HTS films ($\lambda\sim$300 nm, sample linear size is 12 mm by 12 mm). An accurate knowledge of the film thickness and its uniformity are required over the entire sample.

Microwave/millimeter wave reflection/transmission techniques measure S parameters of a coaxial or cylindrical waveguide terminated by the superconductive sample.[12,47–50] The reflection measurements are not suitable to reliably measure an absolute λ. The transmission methods are limited mainly to very thin films of homogeneous thickness and often complicated by a leakage of radiation around the sample.

IR spectroscopy[51] has the advantage of working with very small samples (single crystals), and allows one to estimate all three components of the penetration depth in anisotropic superconductors. However, it is very demanding technically and subject to uncertainty due to the finite frequency measurement range.

3. Probing of internal magnetic field distribution

The muon spin rotation/relaxation (μSR) technique[52–54] has the advantage of being a bulk measurement of λ, but requires a detailed model of the superconducting mixed state. Polarized neutron reflectometry (PNR)[55,56] is sensitive to the shape of the magnetic flux penetration profile itself, rather than just the penetrated magnetic flux. However, even for the best epitaxial HTS films available, the overall surface topology is too poor to obtain λ with sufficient precision.[56]

4. Josephson tunneling

This technique provides an accurate estimation of absolute λ. Its main limitation is the requirement that a Josephson junction be made with the material of interest.

In the present article, we describe the development of a variable spacing parallel plate resonator (VSPPR), first suggested in Ref. 57, which is a Meissner-state resonant technique to obtain the absolute λ. The VSPPR's main novel feature is a continuously variable absolute length scale, the thickness of the dielectric spacer. This allows us to accurately determine the absolute value of λ via continuous measurements of the VSPPR resonant frequency as a function of the dielectric spacer thickness. The technique is quite simple, allows one to investigate both thin films and bulk samples, and provides absolute values for R_s and λ in the same experiment, at the same frequency and temperature. Their extraction from the experimental data is based on a straightforward analytical electrodynamic description of the resonator (and magnetic field penetration into the samples), while no assumptions about the nature of the superconducting state are made. The VSPPR is fully compatible with the conventional parallel plate resonator technique,[29,31,35] which allows one to get the temperature dependence of R_s and λ, so that the full complex conductivity of the superconductor can be constructed.

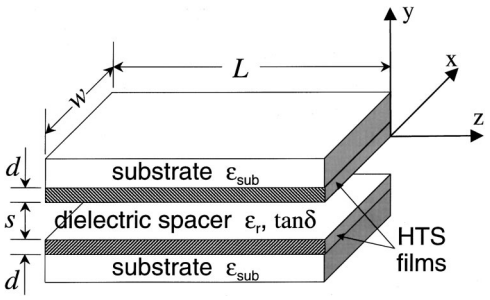

FIG. 1. Geometry of the variable spacing parallel plate resonator. The dielectric spacer is liquid nitrogen or air.

The outline of the article is as follows. After introducing the principle of operation, the experimental setup will be described and experimental results for bulk Cu, and for $YBa_2Cu_3O_7$ and $GdBa_2Cu_3O_7$, thin films will be presented. The values of penetration depth obtained by VSPPR will be compared with the results measured by the mutual inductance technique, and by the conventional PPR technique via a BCS-like fit. The next part of the article is devoted to the error analysis. Finally, a definition for a surface impedance standard based on the VSPPR technique will be proposed. The detailed description of the VSPPR electrodynamics can be found in the Appendix. A preliminary report on this research has appeared elsewhere.[58]

II. PRINCIPLE OF OPERATION

The main idea of our technique is to measure the resonant frequency, *f*, and the quality factor, *Q*, of the VSPPR versus the continuously variable thickness of the dielectric spacer, and to fit them to theoretical forms in order to extract the absolute values of λ and R_s.

The geometry of the VSPPR is shown in Fig. 1. The resonator is formed by two parallel metallic or superconducting plates (bulk material or thin films on dielectric substrates) separated by a thin dielectric spacer, which forms an opened ended transmission line resonator. The spacer is filled by liquid nitrogen or air, which allows us to continuously vary its thickness from contact to several hundred microns. For plates on the order of 1 cm in linear dimension, the resonant frequency of the lowest operating TM_{01} mode is in the range of 10–15 GHz. The full electrodynamic treatment of the VSPPR is given in the Appendix and the main results are presented here.

For the case of superconducting plates, the resonant frequency, f_{SC}, depends on the plates linear dimension *L*, dielectric constant of the spacer $\epsilon=\epsilon_0\epsilon_r$, dielectric spacer thickness *s*, effective penetration depth, $\lambda_{eff}=\lambda\coth(d/\lambda)$, of the electromagnetic field into the superconducting films of finite thickness *d*, and fringe effect:

$$f_{SC}=\frac{f_0}{\sqrt{1+2\lambda_{eff}/s}}\frac{1}{1+\alpha s}, \tag{1}$$

$$f_0=\frac{c}{2L\sqrt{\epsilon_r}}, \tag{2}$$

$$\alpha=\frac{1}{\pi L}\left(0.423+\ln\frac{2}{sf_0\sqrt{\mu_0\epsilon}}\right). \tag{3}$$

Here, f_0 is the resonant frequency of the perfectly conducting VSPPR with no fringe effect and α is the fringe effect geometrical factor. One can see from Eq. (1) that for the spacer thickness $s<(\lambda_{eff}/\alpha)^{1/2}\sim 30\,\mu$m for $\lambda\sim 200$ nm, the penetration depth determines the reduction in the resonant frequency, while for thicker spacers, the resonant frequency is reduced by the fringe effect. Hence, a fit of experimental dependence of $f(s)$ for $s\sim 0$ to 100 μm to Eq. (1) can be used to determine λ_{eff}.

The unloaded *Q* factor of the superconductive VSPPR, Q_{SC}, is determined by ohmic losses in the superconducting films, dielectric losses in the dielectric spacer, and radiation losses:

$$\frac{1}{Q_{SC}}=\frac{1}{Q_\Omega}+\frac{1}{Q_d}+\frac{1}{Q_{rad}}=\frac{R^*_{eff}}{\pi\mu_0 f^*(s+2\lambda_{eff})}\frac{f_{SC}}{f^*}+\tan\delta+\beta s. \tag{4}$$

Here, R^*_{eff} is the effective surface resistance[43] [see Eq. (A6)] at fixed frequency f^*, $\tan\delta$ is the dielectric loss tangent, and $\beta=1/L$ is the radiation geometrical factor. The assumption that $R_s\propto f^2$ for superconductors, i.e., $R_{eff}=R^*_{eff}(f_{SC}/f^*)^2$, is used to derive Eq. (4). Note that Eq. (4) also takes into account the resonator energy stored in both kinetic and geometric inductances of the superconducting plates. For the spacer of thickness $s<(R_{eff}/\pi\mu_0 f\beta)^{1/2}\sim 20\,\mu$m for $R_{eff}\sim 300\,\mu\Omega$, *Q* is determined mainly by the ohmic losses, while for thicker spacers, the radiation losses are dominant. A fit of the experimental dependence $Q(s)$ to Eq. (4) yields the absolute value of R_{eff}.

In the case of the normal metal VSPPR, the resonant frequency, f_{NM}, and *Q* factor, Q_{NM}, are (in the local limit):

$$f_{NM}=\frac{f_0}{\sqrt{1+\delta_{sk}/s}}\left[1-\frac{1}{8}\left(\frac{\delta_{sk}}{s+\delta_{sk}}\right)^2\right]\frac{1}{1+\alpha s}, \tag{5}$$

$$\frac{1}{Q_{NM}}=\frac{\delta_{sk}}{s+\delta_{sk}}+\tan\delta+\beta s, \tag{6}$$

where $\delta_{sk}=\sqrt{2\rho/\omega\mu_0}$ is the skin depth and ρ is the dc resistivity of the normal metal. In Eqs. (5) and (6) δ_{sk} is frequency dependent, i.e., $\delta_{sk}=\delta^*_{sk}\sqrt{f^*/f_{NM}}$. Equation (6) takes into account the resonator energy stored in geometric inductance of the normal metal plates. The frequency and *Q* factor for Cu at room temperature have maximum values at $s\sim(\delta_{sk}/2\alpha)^{1/2}\sim 30\,\mu$m and $s\sim(\delta_{sk}/\beta)^{1/2}\sim 70\,\mu$m, respectively. Fitting of the experimental dependencies for $f(s)$ and $Q(s)$ to the implicit functions (5) and (6) gives us two independent estimates for the absolute skin depth in the normal metal.

III. EXPERIMENTAL SETUP

The VSPPR experimental setup (Fig. 2) consists of a cryogenic linear *Z* stage to move the resonator plates, a films aligner to make them parallel and in-plane aligned, an *in situ*

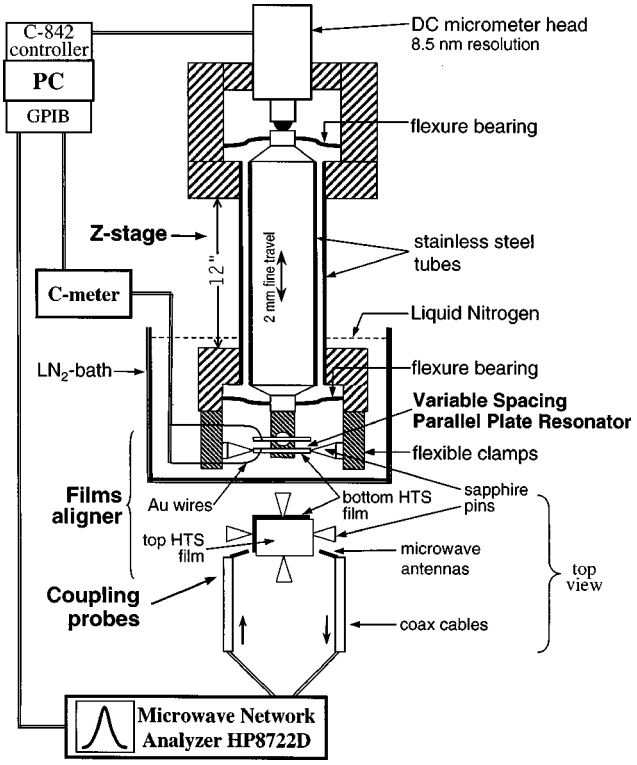

FIG. 2. Schematic of the VSPPR experimental setup (not to scale). The flexible clamp in front of the side view is not shown for clarity.

capacitance micrometry to directly measure the separation and to monitor the parallelism of the plates during the experiment, and microwave coupling probes to excite the resonator.

A. Stage and films aligner

The *Z* stage is based on a home-made slider formed by two coaxial thin-walled stainless-steel tubes with diaphragm-type flexure bearings at the top and bottom ends of the slider. The bearings are made from Be/Cu foil and work at both room and cryogenic temperatures, while eliminating friction and giving high stability. Also they provide a preload for the inner tube translating by the actuator, attached to the top of the slider (Fig. 2). The top of the stage is at room temperature, while the bottom can be immersed into a liquid nitrogen bath. To reduce the effects of thermal contraction, the tubes are made the same length and from the same material. The stage provides about 2 mm of fine rectilinear travel and gives a minimal incremental motion down to 8.5 nm, limited only by the actuator.

The actuator is a commercial motorized micrometer head[59] with a nonrotating ball-shaped tip. It consists of a dc motor with 8.5-nm-resolution rotary encoder driving a precision micrometer screw via a high-ratio backlash-free gear head.

The films aligner consists of two pairs of pins attached to two flexible clamps (Fig. 2). Each of them is made by electrodischarge machining from a single piece of stainless steel. The clamps holding the top and the bottom films are connected to the inner and outer tubes of the slider, respectively. The pins are made from a sapphire stylus inserted into a cylindrical brass housing which is attached to the clamp. Each of the two VSPPR plates is squeezed between a pair of pins and can be finely rotated around the pin-to-pin axis with enough friction to hold the plate in the designated position. Because the rotation axes are perpendicular to each other, a full parallelism of the plates face surfaces can be achieved by bringing them into contact, i.e., they are self-aligning. The aligner also provides an in-plane alignment of the resonator plates.

B. Capacitance measurement of the separation

To perform a precise and accurate *in situ* monitoring of the dielectric spacer thickness (i.e., separation) between the resonator plates, we directly measure a 10 kHz capacitance between them by a precision LCR meter with compensation for stray lead capacitance.[60] To connect each superconducting film to the LCR meter, a 400-μm-wide and 200-nm-thick gold strip on a Cr buffer layer was evaporated through a three-dimensional (3D) shadow mask onto two sides and the edge of the substrate. On the film side of the substrate, the gold contact makes a small pad of area <0.1 mm^2 at one corner, where the microwave current is close to zero. The contact continues over the edge of the substrate and on to the back side, where a strip ~ 7 mm long is deposited. The connection between the strips and the LCR meter leads is done via 50-μm-thick gold wires. A typical VSPPR has a capacitance in the range from 300 to 700 pF at the point of closest approach (depending on the dielectric constant and surface morphology of the samples) down to 8–10 pF at a separation on the order of 100 μm. To determine the spacer thickness, s_c, from the measured capacitance, C, the following expression, taking into account the fringe effects,[61] has been used:

$$C=\epsilon_0\epsilon_r\left\{\frac{Lw}{s_c}+L\left[0.4415+\frac{1}{\pi}\left(\ln\frac{w}{s_c}+1.451\right)\right]+w\left[0.4415+\frac{1}{\pi}\left(\ln\frac{L}{s_c}+1.451\right)\right]\right\}, \tag{7}$$

where L and w are the VSPPR linear dimensions, $\epsilon_0=8.854\times10^{-12}$ F/m, and $\epsilon_r=1.454$ for a liquid nitrogen dielectric spacer.[62] The resolution of the capacitance micrometry is estimated to be much better than the 8.5 nm minimal incremental motion in our setup. The C value measured as a function of the displacement at separations from zero up to several microns is also used to estimate the parallelism of the plates, which is routinely better than 1 mrad.

C. Microwave measurements

The microwave measurements are performed in the undercoupled regime by an HP8722D vector network analyzer (NWA). The built-in -3 dB method is used to determine the resonance frequency and Q factor of the resonator.[63] The coupling probes are two antennas of 8–14 GHz bandwidth connected to the semirigid coaxial cables via a symmetrizing transition.[38,57] They effectively excite the VSPPR due to the similarity of the semicircular shape of the antenna loop and the fringe quasistatic electric field at the resonator edge. The probes provide a variable and contactless coupling to the

TABLE I. Fitting parameters and theoretical predictions for the Cu and HTS VSPPRs: *f* fit—fitting of the frequency vs dielectric spacer thickness data; *Q* fit—fitting of the *Q* factor vs dielectric spacer thickness data; MI—mutual inductance measurements; BCS fit—as described in Sec. V; theory—as described in Sec. II.

		δ_{sk} or λ (nm)					f_0 (GHz)		L (cm)		$R_s(\mu\Omega)$	$1/\beta$ (cm)		s_0 (μm)	
Sample	T (K)	f fit	Q fit	MI	BCS fit	theory	f fit	theory	f fit	theory	Q fit	Q fit	theory	f fit	Q fit
Cu	300	790	770	n/a	n/a	680	12.92	12.52	0.41	1.197	···	1.05	1.197	−1.67	1.51
	77	400	440	n/a	n/a	225	10.80	10.39	0.42	1.197	···	1.09	1.197	−3.49	1.00
YBCO	77	257	n/a	300	···	···	12.55	12.46	0.59	0.998	200	0.35	0.998	−0.38	0.46
GBCO	77	400	n/a	390	344	···	11.45	11.67	1.06	1.065	190	3.3	1.065	2.55	3.33

resonator and allow us to study resonators with Q factors down to 60–70 in the conventional way of measurement, and down to 5–7 by using a unique digital NWA-based procedure developed for investigation of normal metal VSPPRs.[64] The absence of a conductive enclosure in our setup (we use a liquid nitrogen box made of foam plastic), avoids many systematic errors associated with the parasitic ''package modes'' found in conventional parallel plate resonator techniques.[26,34]

D. Experimental procedure

The experimental equipment is run by a personal computer (PC) via GPIB interface, except for the micrometer head which is operated by a PC-board controller.[65] The experimental procedure consists of installation of the samples within the clamps, followed by making them parallel via self-aligning, and testing the parallelism by measuring the capacitance versus displacement at room temperature. Then, in the case of cryogenic measurements, the bottom part of the apparatus is immersed inside a liquid nitrogen bath. Once the samples and the slider have reached thermal equilibrium with the bath, they are brought into contact and self-aligned again. In order to make the plates as close and as parallel as possible, we vibrate the bottom part of the apparatus at a frequency of 2–3 Hz while the plates are in contact. The VSPPR resonant frequency is observed to decrease, and the capacitance to increase. Then the top film is moved away up to 100 μm separation with steps of 10 nm to 1 μm (depending on the separation range) and the resonance frequency and Q factor of the VSPPR versus the displacement are measured.[66] The total time for a single separation measurement is 2–3 s. When the whole run is completed, the films are brought together again in order to check their parallelism.

The experimental setups for the conventional parallel plate resonator and mutual inductance techniques are described in Refs. 31, 35, and 46, respectively.

IV. EXPERIMENTAL RESULTS

To extract the absolute values of λ_{eff} and R_{eff} or δ_{sk} from the experimental data, the latter have to be fit to the theoretical forms (1), (4) for the superconducting VSPPR or (5), (6) for the metallic one.[57] The free parameters are λ_{eff} or δ_{sk}, f_0, and L in the denominator of Eq. (3) for the frequency data, and R_{eff} or δ_{sk} and β for the Q-factor data. Generally, the $\tan\delta$ value cannot be obtained from the fit because $\tan\delta \ll 1/Q$ for air and liquid nitrogen ($\tan\delta = 5\times10^{-5}$) dielectric spacers used here.

In addition, it was found that the following relationship between the exact dielectric spacer thickness, s, in Eqs. (1)–(6) and the capacitively measured separation s_c [see Eq. (7)] must be used:

$$s = s_c + s_0, \tag{8}$$

where s_0 is one more free parameter in the fitting procedure. The nature of this offset will be discussed in Sec. VI B. The parameter values for the fits are summarized in Table I and compared with the theoretical predictions.

A. Normal metal (Cu) VSPPR

To ensure proper operation of the VSPPR technique, normal metal samples with a known value of the microwave skin depth have been investigated. A pair of 0.7-mm-thick OFHC Cu plates with an area of 9.88 by 11.97 mm^2 are used.

Figures 3 and 4 show the resonant frequency and Q factor for the Cu VSPPR as functions of the thickness of air and liquid nitrogen dielectric spacer measured by capacitance micrometry at room and 77.35 K temperatures, respectively. The solid lines are the best fits to Eqs. (5) and (6). There is good agreement between the theory and experiment at small separations where the most important information about the skin depth value is revealed. Some discrepancy at relatively large separations is observed because the fringe effect theory used to derive Eqs. (5) and (6) assumes that the resonator plates have zero thickness and therefore does not provide a good description in the case of thick (i.e., much greater than s) ones serving as a flange for the fringe fields. The precision

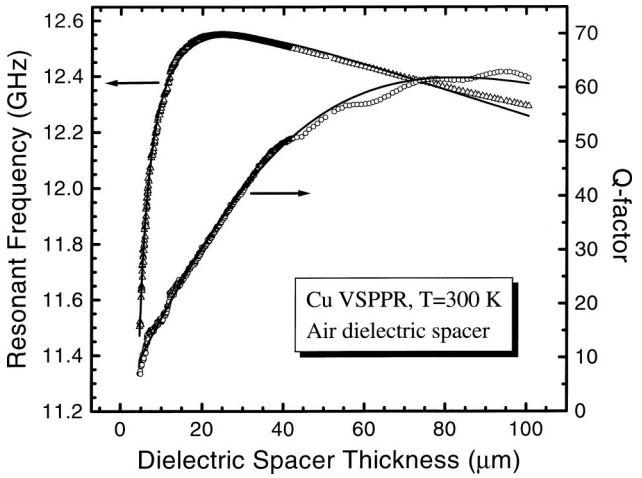

FIG. 3. Cu VSPPR resonant frequency and Q factor vs the dielectric spacer thickness at room temperature. The solid lines are the best fits to Eqs. (5) and (6). Parameter values for the fit are given in Table I.

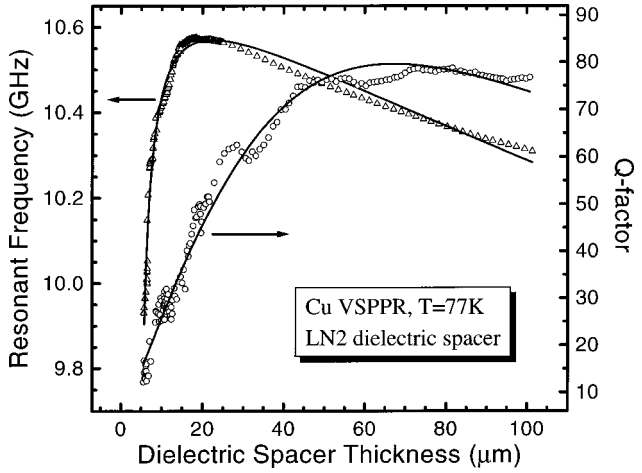

FIG. 4. Cu VSPPR resonant frequency and Q factor vs the dielectric spacer thickness at 77.35 K. The solid lines are the best fits to Eqs. (5) and (6). Parameter values for the fit are given in Table I.

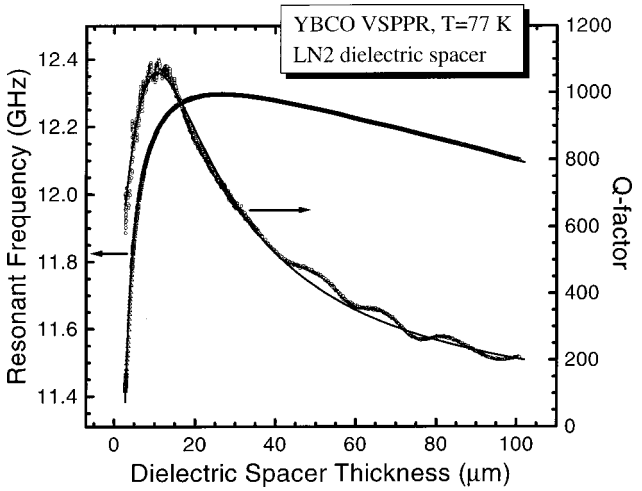

FIG. 5. $YBa_2Cu_3O_7$ VSPPR resonant frequency and Q factor vs the dielectric spacer thickness at 77.35 K. The solid lines are the best fits to Eqs. (1) and (4). Parameter values for the fit are given in Table I.

for determination of the resonant frequency and Q factor of a Cu VSPPR is limited, especially at small separations, by the very low operating Q factor ~ 10. In addition, drift of the digitally subtracted background in the NWA transmission characteristic (see Ref. 64) leads to a degradation of the data obtained at 77.35 K (Fig. 4).

At room temperature, the 10 GHz skin-depth values obtained from the fitting procedures are $\delta_{sk}^{f}=0.79\pm0.1\ \mu$m and $\delta_{sk}^{Q}=0.77\pm0.1\ \mu$m from the frequency and Q-factor data, respectively. The values are close and in good agreement with the theoretical prediction of 0.68 μm based on a Cu electrical resistivity $\rho_{Cu}=1.7\ \mu\Omega$ cm at 20 °C.[62]

The values for the skin depth obtained at liquid nitrogen temperature are $\delta_{sk}^{f}(77\,\mathrm{K})=0.40\pm0.1\ \mu$m and $\delta_{sk}^{Q}(77\,\mathrm{K})=0.44\pm0.1\ \mu$m. The predicted 10 GHz skin depth is 0.225 μm based on a dc resistivity $\rho=0.2\ \mu\Omega$ cm at 77 K,[67] which corresponds to $R_s=8.89\,\mathrm{m}\Omega$. However, at liquid nitrogen temperatures, the microwave skin depth in Cu becomes comparable with the mean free path of conducting electrons,[68] leading to a strong dependence of the surface impedance on surface morphology. Hence, the anomalous skin-effect approach has to be employed in Eqs. (5) and (6), which is beyond the scope of this paper.

B. Superconducting VSPPR

1. $YBa_2Cu_3O_{7-x}$ epitaxial films

The samples are a pair of identical c-axis-oriented $YBa_2Cu_3O_{7-x}$ (YBCO) epitaxial films, grown by metalorganic chemical vapor deposition (MOCVD) on (100)-cut MgO single-crystal dielectric substrates by STI, Inc.,[69] and cut from the same 2-in.-diam wafer. The substrates are 0.5-mm-thick and the resonator effective area is 9.98 by 9.01 mm^2. The YBCO layer has a thickness of 760 ± 30 nm, a critical temperature of 92.4 K, and a transition width of 0.25 K, as measured by ac susceptibility.

Figure 5 shows the experimental dependencies for the resonance frequency and the Q factor of the YBCO VSPPR vs dielectric spacer thickness measured by capacitance micrometry. The operating temperature is 77.35 K and liquid nitrogen is the dielectric spacer. The values obtained are $\lambda_{ab}=257\pm25$ nm and $R_s=200\pm20\ \mu\Omega$ at 10 GHz. No finite thickness correction is necessary, because the film thickness is three times larger than the penetration depth. Extrapolation of the 77 K λ value down to zero temperature via an empirical two fluid model commonly accepted for HTS, $\lambda(T)=\lambda(0)/\sqrt{1-(T/T_c)^2}$, gives $\lambda_{ab}(0)\simeq140$ nm, which is in a good agreement with the literature data for high quality YBCO epitaxial films and crystals.[4,8]

2. $GdBa_2Cu_3O_{7-x}$ epitaxial films

The samples are a pair of nominally identical c-axis-oriented $GdBa_2Cu_3O_{7-x}$ (GBCO) epitaxial films, grown by laser ablation on (100)-cut $LaAlO_3$ single-crystal dielectric substrates by Neocera, Inc.[70] The substrates are 0.6-mm-thick and form a resonator with an area of 10.65 by 7.50 mm^2. The GBCO layer has thickness 300 ± 15 nm, a critical temperature of 92.4 K, and a transition width of 0.3 K, as measured by ac susceptibility.

At the time of the study of the GBCO samples, capacitance micrometry had not yet been introduced into our setup. Hence, the dependencies of the resonance frequency and Q factor for the GBCO films were obtained as functions of the displacement measured by the micrometer head encoder. Several improvements have been made to sufficiently reduce the thermal drift between the micrometer head reading and the actual plate displacement compared to our earlier measurements on these films.[58]

Fitting of the obtained resonance frequency and Q factor dependencies to the forms (1) and (4) gives the effective values $\lambda_{eff}=630\pm80$ nm and 10 GHz $R_{eff}=450\pm60\ \mu\Omega$.[71] The finite thickness correction gives for the intrinsic values $\lambda_{ab}=400\pm40$ nm and $R_s=190\pm20\ \mu\Omega$, which are typical of the literature data for high quality REBaCuO epitaxial films.[4,8]

V. COMPARISON WITH RESULTS OBTAINED BY OTHER TECHNIQUES

The intrinsic ab-plane penetration depths for the YBCO and GBCO films were also measured by the mutual inductance technique at 10 kHz. The values obtained for the two YBCO films are $\lambda_1 = 297 \pm 5$ nm and $\lambda_2 = 304 \pm 10$ nm at 77.35 K. To make a comparison with the raw VSPPR measurements, an average of the two penetration depths has to be made, i.e., $\lambda = (\lambda_1 + \lambda_2)/2 = 300 \pm 15$ nm, which agrees reasonably well with the VSPPR result. The values obtained for the two GBCO films are $\lambda_1 = 377 \pm 11$ nm and $\lambda_2 = 403 \pm 12$ nm at 77.35 K (note that the errors do not include uncertainty in the films thickness). The average of two effective (due to finite film thickness $d = 300$ nm) penetration depths is $\lambda_{\text{eff}} = [\lambda_1 \coth(d/\lambda_1) + \lambda_2 \coth(d/\lambda_2)]/2 = 603 \pm 30$ nm, which agrees with the VSPPR result. Therefore, these results establish that the VSPPR measurement of absolute penetration depth is valid.

The resonance frequency versus temperature for a conventional PPR made from the GBCO films was measured as well.[58] Two 12.5 and 25-μm-thick Teflon™ films are used as dielectric spacers. The fit of the frequency versus temperature data to s-wave BCS theory gives $\lambda_{ab}(0) = 197$ nm and $\lambda_{ab}(77\,\text{K}) = 344$ nm. The latter is close to the VSPPR value. The observed difference may be due to an underestimation of the absolute λ from the temperature fit because of the discrepancy between the data and BCS theory, and uncertainty in the Teflon spacer thickness. It should be pointed out that the dependencies for the change in the effective penetration depth measured at $s_{\text{Teflon}} = 12.5$ and 25 μm agree with each other by assuming that $s = s_{\text{Teflon}} + s^*$, with $s^* \simeq 5$ μm. This value of s^* is on the order of the measured nonflatness of these films, as discussed in Sec. VI A.

VI. DATA FITTING AND EXPERIMENTAL COMPLICATIONS

In Sec. IV, the fitting of experimental data to the theoretical forms (1)–(6) has been used to extract the absolute values of λ_{eff}, R_{eff}, and δ_{sk}. However, in practice, the shapes of the resonator plates and the dielectric spacer are nonideal. Therefore, one has to evaluate the applicability of Eqs. (1)–(6) for describing the real VSPPR and to estimate the errors which these inevitable imperfections introduce into our extraction of λ_{eff}, δ_{sk}, and R_{eff}.

In general, we have found that the accuracy depends mainly on the following three factors: imperfections in the resonator shape, systematic error in capacitance micrometry, and the degree of agreement between the theory and experiment during the fitting procedure. Let us discuss them in more detail.

A. Imperfections in the VSPPR shape

Nonflatness of the resonator plates (films) virtually always appears in practice. For instance, the average nonflatness of commercially available 1 cm^2 single-crystal dielectric substrates for HTS thin films is about 0.5–2 μm, except for $LaAlO_3$ (LAO) which exhibits ~5–10 μm, as a result of going through the irreversible tetragonal-orthorhombic phase transition occurring at $T \sim 500\,^\circ$C after the film deposition process. To image the nonflatness of the samples under study, Newton's rings were studied with a 1/20 wavelength optical flat placed on the top of the film.[72] We observed a bump-like structure of the GBCO/LAO film surfaces with a lateral extent of 5–7 mm and a peak-to-valley height of 5–6 μm. For the Cu plates and YBCO/MgO films, the nonflatness was measured to be less than 5 and 1 μm across the sample, respectively. Note that the thermal contraction between room and cryogenic temperatures and clamping forces may cause additional substrate deformation. Another possible imperfection is tilt of the resonator plates, which may be due to contamination on the plate surfaces and/or torsional deformation of the pins. We find experimentally that the tilt angle in our measurements is routinely less than 1 mrad.

One more imperfection in the VSPPR shape is an in-plane misalignment of the plates due to possible differences in their linear dimensions, their irregular shape, and our inability to make them perfectly aligned during installation into the clamps. An estimate of the misalignment value is $\leqslant 100$ μm for each resonator dimension.

The nonflatness and tilt affect the resonance frequency, Q factor, and ac capacitance of the VSPPR. The in-plane misalignment affects mostly the capacitance micrometry accuracy. Its effect on the resonant frequency is eliminated by using f_0 and L as free fitting parameters, while the ohmic Q factor is shape independent and radiation Q-factor has a fitting parameter β as well.

Note that in the case of a square resonator, a degeneracy between the TM_{01} and TM_{10} modes occurs. In this case, the above imperfections in the resonator shape may provide a coupling between these nominally orthogonal modes, which leads to splitting of the resonant frequencies.[73,74]

B. Modeling of the real VSPPR

To verify the applicability of Eqs. (1)–(4) to extract λ and R_s from experimental data on nonideal VSPPRs, and to estimate the possible errors, a computer modeling of the real experimental situation dealing with a nonflat, tilted or in-plane misaligned VSPPR has been done. First, an electromagnetic model of the distorted VSPPR is created using the approach described below. Next the ''experimental'' dependencies for resonant frequency, Q factor, and capacitance versus geometrical displacement between the resonator plates are generated and these data (i.e., parametric functions) are fit to the forms (1) and (4) and the error in the extracted λ and R_s is analyzed.

One can expect similar influences of nonflatness and tilt on the resonator properties, if they have comparable lateral and vertical geometrical scales. So, here we consider only the tilt of the resonator plates in the planes parallel and perpendicular to the TM_{01} mode propagation direction.

1. Data generation model for tilted resonator

Consider a superconducting VSPPR with in-plane aligned plates having the surface impedance $Z_s = R_s + iX_s$, which are tilted by a small angle $\phi_0 \ll 1$, and ignore the fringe effect. To create an analytical model, a perturbation

technique has to be employed, because the exact solution for such an inclined geometry does not exist for imperfect conductors (except for a special case[75]). Within this approach the relationship between the complex resonant frequency of the superconducting (perturbed) resonator, $\omega_{sc}=\omega'_{sc}+i\omega''_{sc}$, and the resonant frequency of the perfectly conducting resonator of the same shape, ω_{pc}, is[76]

$$\omega_{sc}^2 \simeq \omega_{pc}^2\left(1+i\frac{Z_s}{\Gamma}\right)=\omega_{pc}^2\left(1-\frac{X_s}{\Gamma}+i\frac{R_s}{\Gamma}\right), \tag{9}$$

where $\Gamma=\mu_0\omega_{pc}G$ is the resonator geometrical factor and

$$G=\frac{\int_V|\mathbf{H}|^2dv}{\int_S|H_\tau|^2ds}. \tag{10}$$

Here, $\mathbf{H}$ is the magnetic field calculated (exactly) for the perfectly conducting resonator, and H_τ its tangential component on the resonator walls. The integrals are taken over the whole resonator volume (inclined dielectric spacer) V and the walls (two plates) S. Hence, the dependence on tilt angle ϕ_0 appears in Eq. (10) via the quantities V, $\mathbf{H}$, and H_τ.

An untilted VSPPR has $G=s/2$, and the real part of Eq. (9) is just an expansion of the exact expression (1) for $\lambda/G \ll 1$. So, in order to recover the exact values for the resonant frequency and ohmic Q factor as $\phi_0\to 0$, let us rearrange Eq. (9) as follows:

$$\omega'_{sc}=\frac{\omega_{pc}}{\sqrt{1+\lambda/G}}, \tag{11}$$

$$Q_\Omega^{-1}=\frac{2\omega''_{sc}}{\omega'_{sc}}=\frac{R_s}{\mu_0\omega'_{sc}(G+\lambda)}. \tag{12}$$

The capacitance to be ''measured'' by capacitance micrometry is approximated as $C=\int_A(\epsilon_0\epsilon_r/s_{nu})da$, where s_{nu} is the nonuniform dielectric spacer thickness, the integral is taken over the resonator area A, and the capacitive dielectric spacer s_c is given by Eq. (7). In order to fit the generated data to the forms (1) and (4), a linear relationship between s and s_c has been used as in Eq. (8).

2. Tilt in the plane parallel to the mode propagation direction

Let us put the cylindrical coordinates so that the z axis is perpendicular to the direction of the mode propagation, r, and parallel to the resonator plates. The magnetic field of the perfectly conducting resonator in Eq. (10) has only a z component[77] $H_z(r)=B_1H_0^{(1)}(kr)+B_2H_0^{(2)}(kr)$, where $H_0^{(1)}(kr)$ and $H_0^{(2)}(kr)$ are the Hankel functions of a first and second kind, respectively, k is the wave number in the dielectric, and B_1 and B_2 are constants. The procedure described in Sec. VI B 1 has been performed for a VSPPR of area 1 cm^2 and penetration depth of 250 nm. It is found that in order to obtain an error in λ of less than 10%, the tilt angle has to be less than 0.7 mrad. This tilt gives an overestimation of λ and a negative offset value $|s_0|\leqslant 1.2\ \mu$m.

3. Tilt in the plane perpendicular to the mode propagation direction

The cylindrical coordinates are chosen so that the z axis is parallel to the direction of the mode propagation. The magnetic field in Eq. (10) has only an r component. Based on the law of magnetic flux conservation it is $H_r(r,z)=D\sin(\pi z/L)/\phi_0 r$, where D is constant. For the same resonator as above, it is found that an error in λ of less than 10% is obtained if this type of tilt is less than 1 mrad. This gives underestimation of λ and a negative offset value $|s_0|\leqslant 1.7\ \mu$m.

C. Accuracy of capacitance micrometry

While the precision of the capacitance micrometry is well above the requirements of our experiment, a systematic error in the capacitance value may noticeably contribute to the error in λ. By performing the modeling of an untilted VSPPR, as discussed at the beginning of Sec. VI B, we found that our estimated in-plane misalignment $\sim 100\ \mu$m for each resonator dimension gives an error in absolute λ on the order of 2%. The estimate for systematic error in the capacitance value due to imperfect compensation of the stray capacitance for the LCR meter leads and/or uncertainty in the dielectric spacer permittivity (in the case of liquid nitrogen) is $\leqslant 2$ pF, which gives an error in λ less than 6%.

To conclude this section, the three most common forms of VSPPR nonideality and systematic error in capacitance micrometry give rise to errors in absolute λ on the order of 10% or less for our experimental conditions.

D. Microwave coupling

We observed that strong coupling between the antennas and VSPPR may lead to some disagreement between the experimental data and the theory during the fitting procedure. Strong coupling distorts the resonator eigenfrequency and Lorentzian shape of the resonance curve due to the interaction between electromagnetic oscillations in the resonator and standing waves in the coax cables. This interaction is stronger when the VSPPR and the standing wave resonances have comparable bandwidths. Another possible parasitic effect is the increase of the coupling as the plates separation increases. To eliminate the influence of these effects on the accuracy of the experiment, the coupling has to be minimized such that the insertion loss of the VSPPR is at least 35–40 dB.

E. Discussion of the secondary fitting parameters

Let us discuss the secondary fitting parameters from Table I, such as the frequency of the perfectly conducting VSPPR with no fringe effect, f_0, fringe effect factors L and β, and offset in the dielectric spacer thickness s_0.

The discrepancy between the theoretical predictions and fitting values obtained for f_0 may be due to the following factors: in-plane misalignment of the resonator plates; disagreement between the experimental data and theory at large separations for the Cu VSPPR (see Sec. IV); the edges of the Cu plates are not perfectly square-shaped (unlike the HTS

films on single-crystal substrates), which causes the effective resonator length to be slightly shorter than the geometrical one; error in the value for microwave dielectric permittivity of liquid nitrogen.

The fitting parameters L and $1/\beta$ are usually smaller than the predicted ones, which corresponds to an underestimate of the fringe effect geometrical factors from the theory (see Appendix) used to derive Eqs. (1)–(6).

The s_0 values obtained from the frequency fits are on the order of -1 μm (except for the GBCO VSPPR, where the capacitance micrometry was not employed), which agrees with the results of simulation for the tilted VSPPR discussed above in Sec. VI B.

VII. R_s STANDARD

Establishment of a surface resistance standard is an important issue for HTS film applications in wireless communications. Currently, there are two techniques,[14] namely, a (conventional) parallel plate resonator and a dielectric resonator,[78] as contestants in the race to become a standard for characterization of HTS films for microwave applications. We believe that the VSPPR technique can fill this role as well. The definition can be done in terms of a frequency and a length: an effective surface resistance of 100 $\mu\Omega$ at 10 GHz is a FWHM=2.533 MHz of the resonance curve for the ohmic Q factor produced by the VSPPR with an effective separation between the plates $s_{\text{eff}}=s+2\lambda_{\text{eff}}=10$ μm. Note that the VSPPR's ohmic Q factor (and so the FWHM above) is independent of the sample geometry and mode number.

VIII. FUTURE WORK

For the future, we are planning to develop a version of the VSPPR for operation at liquid helium temperature. The use of flexure bearings and direct capacitance micrometry eliminates the influence of the cryogenic environment on the performance of the system, and allows the existing micropositioning setup to be adapted for 4.2 K operation. An active film aligner could decrease the tilt and enhance the accuracy of the technique. To improve the performance of the fitting procedure, a 3D electromagnetic simulation of the real VSPPR (including substrates) followed by the development of analytical calculations for the resonant frequency, Q factor, and ac capacitance has to be done.

ACKNOWLEDGMENTS

This material is based upon work supported by the North Atlantic Treaty Organization under Grant No. DGE-9710702 awarded in 1997, by the National Science Foundation under Grant No. DMR-9624021, and by the Maryland Center for Superconductivity Research. The authors are thankful to R. Wood of UMD and R. Belov and V. Markelov of IPM RAS for fruitful discussions about the experimental setup, J. Musolf of STI and H. Christen, S. Green, H. Harshevarden, and A. Pique of Neocera, Inc. for HTS samples, A. Schwartz and B. J. Feenstra for very helpful attention paid to this work, A. Vostrukhov for discussions about the nonflatness issue, A. Nielsen for advice about the contacts, and J. Halbritter and N. Bontemps for critical comments on the article.

APPENDIX: ELECTRODYNAMICS OF THE VSPPR

Let us briefly outline the derivation of Eqs. (1)–(6) based on the results of several works[37–39,57,68,79,80] on the electrodynamics of the superconducting and metallic parallel plate transmission lines and resonators. Because the final results for the resonant frequency and Q factor are used for extraction of numerical values from the experimental data, only terms with accuracy up to 10^{-4} for the resonant frequency and 10^{-2} for the Q factor will be kept.

1. Propagation and attenuation constants in a parallel plate transmission line

The transmission line geometry is shown in Fig. 1. Two superconductive or metallic plates of thickness d and width w are separated by a dielectric spacer of thickness s ($s \ll w$) with complex permittivity $\epsilon=\epsilon_0\epsilon_r(1-i\tan\delta)$ and permeability $\mu=\mu_0$. In the case of $|ks|\ll 1$ ($k=\omega\sqrt{\mu\epsilon}$ is the complex wave number of the dielectric), only the slow-wave fundamental TM mode exists between the plates. Let all fields vary as $\exp[i(\omega t-hz)]$, where $h=h_1-ih_2$ is the complex longitudinal wave number. Solution of Maxwell's equations in the space between the plates together with the Leontovich impedance boundary condition[81] applied at the plates surface

$$Z_{\text{eff}}=R_{\text{eff}}+iX_{\text{eff}}=\left(\frac{E_z}{H_x}\right)_{y=0}=-\left(\frac{E_z}{H_x}\right)_{y=-s} \tag{A1}$$

yields the dispersion relation for the TM mode:[38,79]

$$\omega\epsilon Z_{\text{eff}}=-ig\tan\frac{gs}{2}, \tag{A2}$$

where Z_{eff} is the effective surface impedance of the plate, and $g=\sqrt{k^2-h^2}$ is the transverse wave number. Because $|Z_{\text{eff}}|\ll|\sqrt{\mu_0/\epsilon}|$ and $|ks|\ll 1$, the expansion of Eq. (A2) yields

$$h^2=k^2\left(1-i\frac{2Z_{\text{eff}}}{\mu_0\omega s}\right). \tag{A3}$$

Note that the accuracy of Eq. (A3) is on the order of $|Z_{\text{eff}}\sqrt{\mu_0/\epsilon}|^2\ll 10^{-4}$ for any actual experimental situation.

Separation of the real and imaginary parts in Eq. (A3) gives the propagation and attenuation constants:

$$h_1^2=k_0^2\epsilon_r\left(1+\frac{2X_{\text{eff}}}{\mu_0\omega s}\right)\times\left\{\frac{1}{2}+\sqrt{\frac{1+\tan^2\delta}{4}\left[1+\left(\frac{2R_{\text{eff}}}{\mu_0\omega s+2X_{\text{eff}}}\right)^2\right]}-\frac{R_{\text{eff}}\tan\delta}{\mu_0\omega s+2X_{\text{eff}}}\right\}, \tag{A4}$$

$$h_2=\frac{k_0^2\epsilon_r}{2h_1}\left(1+\frac{2X_{\text{eff}}}{\mu_0\omega s}\right)\left(\frac{2R_{\text{eff}}}{\mu_0\omega s+2X_{\text{eff}}}+\tan\delta\right), \tag{A5}$$

where $k_0=\omega\sqrt{\epsilon_0\mu_0}$ is the vacuum wave number. Note that the term in figure parenthesis in Eq. (A4) is correction to the propagation constant due to finite ohmic and dielectric losses.

2. Superconducting transmission line

The effective surface impedance of a finite thickness superconducting plate (film) of intrinsic impedance $Z_s=R_s+iX_s$ on a dielectric substrate of impedance $Z_{\rm sub}$ within the approach $R_s\ll X_s$ and $d\gg\lambda X_s/Z_{\rm sub}$ is[43]

$$R_{\rm eff}=R_s\left[\coth(d/\lambda)+\frac{d/\lambda}{\sinh^2(d/\lambda)}\right]+\frac{X_s^2}{Z_{\rm sub}}\frac{1}{\sinh^2(d/\lambda)}, \tag{A6}$$

$$X_{\rm eff}=X_s\coth(d/\lambda)=\mu_0\omega\lambda_{\rm eff}. \tag{A7}$$

A high quality superconducting film of thickness $d\gg\lambda X_s/Z_{\rm sub}$ at temperatures $T<0.95\,T_c$ and frequencies <50 GHz exhibits $R_{\rm eff}/X_{\rm eff}\ll 1 (R_{\rm eff}/X_{\rm eff}=2R_s/X_s$ for $d\ll\lambda)$, and typically $\tan\delta\leqslant 10^{-3}$, so within the accuracy stated above Eqs. (A4) and (A5) yield

$$h_1=k_0\sqrt{\epsilon_r}\sqrt{1+\frac{2\lambda_{\rm eff}}{s}}, \tag{A8}$$

$$h_2=\frac{k_0\sqrt{\epsilon_r}}{2}\sqrt{1+\frac{2\lambda_{\rm eff}}{s}}\left(\frac{2R_{\rm eff}}{\omega\mu_0(s+2\lambda_{\rm eff})}+\tan\delta\right). \tag{A9}$$

The loss correction in h_1 is omitted, which is valid for experimentally observed quality factors greater than 100.

3. Normal metal transmission line

For the thick ($d\gg\delta_{\rm sk}$) metallic plate, $Z_{\rm eff}=\mu_0\omega\delta_{\rm sk}(1+i)/2$ in the local limit, where $\delta_{\rm sk}$ is the skin depth. Because the minimum measurable Q factor is $\geqslant 5$ [i.e., $\delta_{\rm sk}(s+\delta_{\rm sk})\geqslant 5$] in our experiment and $\tan\delta\leqslant 10^{-3}$, an expansion can be employed in Eq. (A4), which gives

$$h_1=k_0\sqrt{\epsilon_r}\sqrt{1+\frac{\delta_{\rm sk}}{s}}\left[1+\frac{1}{8}\left(\frac{\delta_{\rm sk}}{s+\delta_{\rm sk}}\right)^2\right], \tag{A10}$$

$$h_2=\frac{k_0\sqrt{\epsilon_r}}{2}\sqrt{1+\frac{\delta_{\rm sk}}{s}}\left[\frac{\delta_{\rm sk}}{s+\delta_{\rm sk}}+\tan\delta\right]. \tag{A11}$$

4. Reflection from the open edge of the semi-infinite transmission line

The VSPPR has open ends, in contrast with the infinite line discussed above. Hence, it is important to consider the fringe effects. The exact solution for the TEM mode complex reflection coefficient

$$R=-|R|\exp(-i\Theta) \tag{A12}$$

from the edge of a semi-infinite perfectly conducting parallel plate transmission line made from plates of zero thickness, in the case of $ks\ll 1$ gives[82]

$$|R|=\exp\left(-\frac{ks}{2}\right)\simeq 1-\frac{ks}{2}, \tag{A13}$$

$$\Theta=\frac{ks}{\pi}\left(1-0.5772+\ln\frac{4\pi}{ks}\right). \tag{A14}$$

These expressions are valid for the situation where the dielectric is the same inside and outside of the line and for infinitely wide plates.

5. Superconducting and metallic VSPPRs

The complex resonance condition for a resonator of length L is[82]

$$\exp(-ihL)=R. \tag{A15}$$

Substitution of Eqs. (A12)–(A14) and the complex angular frequency $\omega=\omega'+i\omega''$ into Eq. (A15) and separation of real and imaginary parts yields

$$h_1(\omega')L+\Theta(\omega')=\pi, \tag{A16}$$

$$2h_2(\omega')L+s\omega'\sqrt{\mu_0\epsilon_0\epsilon_r}=\pi Q^{-1}, \tag{A17}$$

where the resonant frequency is defined as $\omega'/2\pi$, and the Q factor is $\omega'/2\omega''$.

For a superconducting VSPPR, substitution of Eqs. (A8), (A9) into (A16), (A17) gives us Eqs. (1)–(3) for the resonant frequency, $f_{\rm SC}$. Equation (4) is obtained for the Q factor, $Q_{\rm SC}$, ignoring the energy stored in the fringe fields. This contribution is on the order of $s/L\leqslant 10^{-2}$. A similar procedure applied to the normal metal VSPPR by means of Eqs. (A10) and (A11) for the longitudinal wave number, h, yields Eqs. (5) and (6).

It is important to discuss the applicability of Eqs. (1)–(6) for the description of the actual VSPPR of finite width $w\gg s$. The effects of the finite width on the propagation constant (A4) and the ohmical Q factor, can be estimated using Wheeler's principle[61] as $\lambda[\delta_{\rm sk}]/w\leqslant 10^{-4}$ and $s/w\leqslant 10^{-2}$, respectively. This is within the accuracy stated above. For the fringe effect terms in Eqs. (1)–(6), it can be shown that in the case of $w\gg s$, the finite width of the line affects (in the first approach) only the numerical values, but not the linear form of $|R|$ and Θ dependencies (A13), (A14) on s.[61,83] The power radiated from the side edges of the VSPPR depends linearly on s as well. Hence, such effects can be absorbed in the fitting procedure by the free parameters L and β (see Table I).

[1] A. B. Pippard, Proc. R. Soc. London, Ser. A **191**, 399 (1947); **203**, 98 (1950).
[2] J. G. Bednorz and K. A. Muller, Z. Phys. B: Condens. Matter **64**, 189 (1986).
[3] M. K. Wu, J. R. Asburn, C. J. Torng, P. H. Nor, R. L. Meng, L. Gao, Z. J. Huang, and C. E. Chu, Phys. Rev. Lett. **58**, 908 (1987).
[4] N. Newman and W. G. Lyons, J. Supercond. **6**, 119 (1993).
[5] Z.-Y. Shen, *High-Temperature Superconducting Microwave Circuits* (Artech House, Boston, 1994).
[6] M. A. Hein, in *Studies of High Temperature Superconductors*, Vol. 18, edited by A. Narlikar (Nova Science Publishers, New York, 1996), pp. 141–216.
[7] A. P. Mourachkine and A. R. Barel, Ref. 6, Vol. 17, pp. 222–246.
[8] D. A. Bonn and W. N. Hardy, in *Physical Properties of High Temperature Superconductors V*, edited by D. M. Ginsberg (World Scientific, Singapore, 1996), pp. 9–97.
[9] M. R. Trunin, J. Supercond. **11**, 381 (1998).
[10] D. C. Mattis and J. Bardeen, Phys. Rev. **111**, 412 (1958).

[11] P. J. Hirshfield, W. O. Putikka, and D. J. Scalapino, Phys. Rev. B **50**, 10250 (1994).
[12] R. C. Taber, P. Merchant, R. Hiskes, S. A. DiCarolis, and M. Narbutovskih, J. Supercond. **5**, 371 (1992).
[13] A. R. Jha, *Superconductor Technology* (Wiley, New York, 1998).
[14] J. Mazierska, J. Supercond. **10**, 73 (1997).
[15] M. Tinkham, *Introduction to Superconductivity*, 2nd ed. (McGraw–Hill, New York, 1996), p. 106.
[16] B. W. Langley, S. M. Anlage, R. F. W. Pease, and M. R. Beasley, Rev. Sci. Instrum. **62**, 1801 (1991).
[17] L. Krusin-Elbaum, R. L. Greene, F. Holtzberg, A. P. Malozemoff, and Y. Yeshurun, Phys. Rev. Lett. **62**, 217 (1989).
[18] S. Shridar, D.-H. Wu, and W. L. Kennedy, Phys. Rev. Lett. **63**, 1873 (1989).
[19] N. Klein, G. Muller, H. Piel, B. Roas, L. Shultz, U. Klein, and M. Peininger, Appl. Phys. Lett. **54**, 757 (1989).
[20] N. Klein *et al.*, J. Supercond. **5**, 195 (1992).
[21] C. Wilker, Z.-Y. Shen, V.-X. Nguen, and M. S. Brenner, IEEE Trans. Appl. Supercond. **3**, 2832 (1992).
[22] Y. Kobayashi and H. Yoshikawa, IEEE Trans. Microwave Theory Tech. **46**, 2524 (1998).
[23] D. E. Oates, A. C. Anderson, and P. M. Mankiewich, J. Supercond. **3**, 251 (1990).
[24] S. M. Anlage, H. Sze, H. J. Snortland, S. Tanaka, B. Langley, C.-B. Eom, M. R. Beasley, and R. Taber, Appl. Phys. Lett. **54**, 2710 (1989).
[25] J. M. Pond, K. R. Carrol, J. S. Horwitz, D. B. Chirsey, M. S. Osofsky, and V. C. Cestone, Appl. Phys. Lett. **59**, 3033 (1991).
[26] R. C. Taber, Rev. Sci. Instrum. **61**, 2200 (1990).
[27] S. A. Reible and C. W. Wilker, IEEE Trans. Magn. **27**, 2813 (1991).
[28] A. Vogt, T. Scherer, M. Neuhaus, and W. Jutzi, Proceedings of V German-CIS Bilateral Seminar on High-Temperature Superconductivity, Kloster-Banz, 5–9 October 1992.
[29] M. S. Pambianchi, D. H. Wu, L. Ganapathi, and S. M. Anlage, IEEE Trans. Appl. Supercond. **3**, 2774 (1993).
[30] M. Golosovsky, M. Tsindleht, H. Chayet, and D. Davidov, Phys. Rev. B **50**, 470 (1994).
[31] M. S. Pambianchi, S. M. Anlage, E. S. Hellman, E. H. Hartford, M. Bruns, and S. Y. Lee, Appl. Phys. Lett. **64**, 244 (1994).
[32] I.-S. Kim, K. W. Lee, Y. K. Park, and J.-C. Park, Jpn. J. Appl. Phys., Part 1 **34**, 590 (1995).
[33] R. Perez, T. Tybell, M. Decroux, J. M. Triscone, and O. Fischer, Chechoslovac J. Phys. **46**, 1081 (1996).
[34] F. Gao, M. V. Klein, J. Kruse, and M. Feng, IEEE Trans. Microwave Theory Tech. **44**, 944 (1996).
[35] L. V. Mercaldo, S. M. Anlage, and L. Maritato, Phys. Rev. B **59**, 4455 (1999).
[36] G. Dahlinger, G. Godel, J. Hasse, N. Geng, W. Wiesbeck, and J. Halbritter (unpublished).
[37] Z. Ma, Ph.D. thesis, Stanford University, 1995.
[38] V. V. Talanov, Ph.D. thesis, Institute for Physics of Microstructures of the Russian Academy of Sciences, Nizhny Novgorod, 1997.
[39] J. C. Swihart, J. Appl. Phys. **32**, 461 (1961).
[40] W. Rauch, E. Gornik, G. Solkner, A. A. Valenzuela, F. Fox, and H. Behner, J. Appl. Phys. **73**, 1866 (1993).
[41] A. Porch, M. J. Lancaster, and R. G. Humphreys, IEEE Trans. Microwave Theory Tech. **43**, 306 (1995).
[42] C. B. Eom *et al.*, Physica C **171**, 354 (1990).
[43] N. Klein, H. Chaloupka, G. Muller, S. Orbach, H. Piel, B. Roas, L. Schultz, U. Klein, and M. Peiniger, J. Appl. Phys. **67**, 6940 (1990).
[44] A. T. Fiory, A. F. Hebard, P. M. Makiewich, and R. E. Howard, Appl. Phys. Lett. **52**, 2165 (1988).
[45] S. J. Turneaure, E. R. Ulm, and T. R. Lemberger, J. Appl. Phys. **79**, 4221 (1996).
[46] J. H. Claassen, M. L. Wilson, J. M. Byers, and S. Adrian, J. Appl. Phys. **82**, 3028 (1997).
[47] J. Booth, D. H. Wu, and S. M. Anlage, Rev. Sci. Instrum. **65**, 2082 (1994).
[48] F. Miranda, W. L Gordon, K. B. Bhasin, V. O. Heinen, and J. D. Warner, J. Appl. Phys. **70**, 5450 (1991).
[49] B. J. Feenstra, F. C. Klaassen, D. van der Marel, Z. H. Barber, R. Perez Pinaya, and M. Decroux, Physica C **278**, 213 (1997).
[50] L. A. de Vaulchier, J. P. Vieren, Y. Guldner, N. Bontemps, R. Combescot, Y. Lemaitre, and J. C. Mage, Europhys. Lett. **33**, 153 (1996).
[51] D. N. Basov, R. Liang, D. A. Bonn, W. N. Hardy, B. Dabrowski, M. Quijada, D. B. Tanner, J. P. Rice, D. M. Ginsberg, and T. Timusk, Phys. Rev. Lett. **74**, 598 (1995).
[52] T. Forgan, Nature (London) **329**, 483 (1987).
[53] Y. J. Uemura *et al.*, Phys. Rev. B **38**, 909 (1988).
[54] D. R. Harshman *et al.*, Phys. Rev. B **39**, 851 (1989).
[55] R. Felici, J. Penfold, R. C. Ward, E. Olsi, and C. Matacotta, Nature (London) **329**, 523 (1987).
[56] Huai Zhang, J. W. Lynn, C. F. Majkrzak, S. K. Satija, J. H. Kang, and X. D. Wu, Phys. Rev. B **52**, 10395 (1995).
[57] A. Ya. Basovich, R. K. Belov, V. A. Markelov, L. A. Mazo, S. A. Pavlov, V. V. Talanov, and A. V. Varganov, J. Supercond. **5**, 497 (1992).
[58] V. V. Talanov, L. V. Mercaldo, and S. M. Anlage, IEEE Trans. Appl. Supercond. **9**, 2179 (1999).
[59] M-224.50 DC-Mike Drive, Physik Instrumente (PI) GmbH & Co., Waldbronn, Germany.
[60] SR720 LCR Meter, Stanford Research Systems, Inc., Sunnyvale, CA.
[61] K. C. Gupta, R. Garg, I. Bahl, and P. Bhartia, *Microstrip Lines and Slot Lines*, 2nd. ed. (Artech House, Boston, 1996).
[62] *CRC Handbook of Chemistry and Physics*, 70th ed. (CRC, Boca Raton, FL, 1989–1990).
[63] P. J. Petersan and S. M. Anlage, J. Appl. Phys. **84**, 3392 (1998).
[64] The digital subtraction of background is accomplished as follows: first, at the point of conducting contact between the plates (i.e., at zero separation) the $|S_{21}|$ vs frequency sweep is averaged and put into the NWA's memory. Then the NWA is switched to measure ''data−memory'' (i.e., the actual transmission characteristic with subtracted nonresonant background), and the top resonator plate is moved away. Averaging and smoothing are applied to the displayed ''data−memory'' characteristic and the resonance frequency and Q factor are measured by the built-in -3 dB method.
[65] C-842.20 DC-motor controller, Physik Instrumente (PI) GmbH & Co., Waldbronn, Germany.
[66] To synchronize the microwave and capacitance data at each separation, we use an internal averaging of the capacitance by the LCR meter during the time of the S_{21} vs frequency sweep by the NWA.
[67] N. W. Ashcroft and N. D. Mermin, *Solid State Physics* (Holt, Rinehart and Winston, New York, 1976), p. 8.
[68] R. E. Matick, *Transmission Lines for Digital Communication Networks* (McGraw–Hill, New York, 1969), Chap. 6.
[69] J. Musolf, J. Alloys Compd. **251**, 292 (1997); J. Musolf and E. J. Smith, IEEE Trans. Appl. Supercond. **9**, 2167 (1999).
[70] T. Venkatesan and S. M. Green, The Industr. Physicist **2**, 22 (1996).
[71] A preliminary result of $\lambda_{\text{eff}} \simeq 2\ \mu$m and $R_{\text{eff}} = 530\ \mu\Omega$ presented in Ref. 58 for the GBCO films was done in the absence of capacitance micrometry, hence the performance of the experimental setup at that time had been affected by thermal drift.
[72] Yu. N. Nozdrin, Institute for Physics of Microstructures RAS, Nizhny Novgorod (personal communication).
[73] A. V. Vostrukhov, M. S. thesis, Nizhny Novgorod State University, 1999.
[74] A. V. Vostrukhov, V. V. Talanov, R. K. Belov, and S. A. Pavlov (unpublished).
[75] An exact solution via the product exists for inclined geometry only for the case of inhomogeneous surface reactance, see V. I. Talanov, Izvestia Vuzov Radiofizika **2**, 132 (1959).
[76] L. A. Weinstein, *Electromagnetic Waves* (Radio i svyaz', Moscow, 1988), p. 364.
[77] S. Ramo, J. R. Whinnery, and T. V. Duzer, *Fields and Waves in Communication Electronics* (Wiley, New York, 1984), p. 466.
[78] R. Ono, NIST, Boulder, CO (personal communication).
[79] P. V. Mason and R. W. Gould, J. Appl. Phys. **40**, 2039 (1969).
[80] F. Abbas and L. E. Davis, Int. J. Electron. **77**, 481 (1994).
[81] M. A. Leontovich, *Investigations of Radiowave Propagation* (Academy of Sciences, Moscow, 1948), Chap. 2.
[82] L. A. Weinstein, *Theory of Diffraction and Method of Factorization* (Sovetskoe Radio, Moscow, 1966).
[83] V. V. Talanov (unpublished).